Electronic Properties of a Graphene Device with Peptide Adsorption: Insight from Simulation

Brahim Akdim,[†,*] Ruth Pachter,[*,†] Steve S. Kim,[†] Rajesh R. Naik,[†] Tiffany R. Walsh,[‡] Steven Trohalaki,[†] Gongyi Hong,[†] Zhifeng Kuang,[†] and Barry L. Farmer[†]

[†]Air Force Research Laboratory, Materials & Manufacturing Directorate, Wright-Patterson Air Force Base, Ohio 45433, United States
[‡]Institute for Frontier Materials, Deakin University, Waurn Ponds, Victoria 3216, Australia

Ⓢ *Supporting Information*

ABSTRACT: In this work, to explain doping behavior of single-layer graphene upon HSSYWYAFNNKT (**P1**) and HSSAAAAFNNKT (**P1−3A**) adsorption in field-effect transistors (GFETs), we applied a combined computational approach, whereby peptide adsorption was modeled by molecular dynamics simulations, and the lowest energy configuration was confirmed by density functional theory calculations. On the basis of the resulting structures of the hybrid materials, electronic structure and transport calculations were investigated. We demonstrate that $\pi-\pi$ stacking of the aromatic residues and proximate peptide backbone to the graphene surface in **P1** have a role in the p-doping. These results are consistent with our experimental observation of the GFET's p-doping even after a 24-h annealing procedure. Upon substitution of three of the aromatic residues to Ala in (**P1−3A**), a considerable decrease from p-doping is observed experimentally, demonstrating n-doping as compared to the nonadsorbed device, yet not explained based on the atomistic MD simulation structures. To gain a qualitative understanding of **P1−3A**'s adsorption over a longer simulation time, which may differ from aromatic amino acid residues' swift anchoring on the surface, we analyzed equilibrated coarse-grain simulations performed for 500 ns. Desorption of the Ala residues from the surface was shown computationally, which could in turn affect charge transfer, yet a full explanation of the mechanism of n-doping will require elucidation of differences between various aromatic residues as dependent on peptide composition, and inclusion of effects of the substrate and environment, to be considered in future work.

KEYWORDS: *field effects transistor, peptide adsorption, single-layer graphene, density functional theory, molecular dynamics, electronic properties*
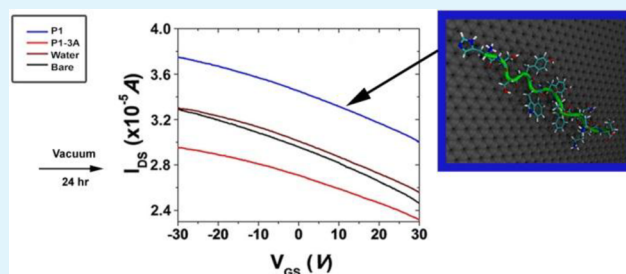
1. INTRODUCTION

It has been postulated that the experimentally measured response of single-layer graphene field-effect transistors (GFETs) is weaker than expected[1] because the electronic properties can be greatly perturbed by impurities such as the substrate and environment, among other potential limiting factors.[2] Theoretically, the role of impurities and scatterers was analyzed in some cases[3,4] and such interactions were also the topic of simulations.[5−7] Indeed, delineating the intrinsic performance of a GFET has been challenging, requiring special procedures and analysis. For example, devices with graphene fabricated by chemical vapor deposition (CVD) demonstrated improved mobility after treatment by a buffered oxide etch, noting that H_2O/O_2 was the primary reason for p-type doping.[8] The mobility of CVD grown graphene on SiO_2 can also be limited by water molecules trapped between the graphene and substrate, requiring careful control of the device's fabrication.[9] This was analyzed in terms of the supposition that the mobility μ and impurity density is a constant,[10] namely $\mu n_0 \approx 1.5 \times 10^{15}/(V\ s)$, with n_0/n_{imp} of ca. 0.2−0.5 on SiO_2.[9] Effects of oxygen plasma were also investigated.[11] *n*-Type behavior of a

device after long-term (20h) degassing in vacuum at 200 °C was demonstrated,[12] explained theoretically by a surface state density below the conduction band edge that donates electrons to the graphene sheet to balance the chemical potential. In recent work on chemical sensing in GFETs, it was suggested that defects in the underlying SiO_2 result in p-doping of the device.[13] A combination of annealing and wet-chemical treatment with chloroform were needed for improved performance of such devices.[14] As pointed out by Nagashio et al.,[15] scattering centers at the SiO_2−graphene interface can be attributed to negatively charged silanol groups of the SiO_2 substrate.

Inclusion of biological adsorbates further complicates the device's behavior. Although the recent advent in development of biofunctional GFETs holds great promise for sensitive and selective detection of chemical and biological analytes,[16,17] thus moving beyond detection of gas molecules,[18] understanding of

the intrinsic response of the device upon biomolecular adsorption is difficult. For example, substrate interactions and surface adsorbates were found to contribute to charge noise in carbon nanotube-based biosensors.[19] Therefore, explaining the intrinsic response of a GFET upon peptide adsorption is desirable. This can be accomplished by comparison of pristine and peptide-adsorbed GFETs, reducing the requirement for analysis of environmental scatterers.

Peptide-GFETs previously fabricated by Kim et al.[20] demonstrated enhanced p-type doping of graphene via adsorption of the peptide HSSYWYAFNNKT (denoted **P1** herein). This carbon nanotube binding peptide, identified from combinatorial phage display,[21] showed preferential binding on the basal plane of graphene. Compared to a graphene edge-binding peptide, **P1** exhibited >40 times faster binding kinetics, attributed to $\pi-\pi$ interactions resulting from stacking of the aromatic rings on the graphene surface.[20] Thus, **P1** was chosen as a robust binder selective to graphene in this work. For comparison, another dodecapeptide, where three of the aromatic residues were changed to Ala was investigated, i.e., HSSAAAAFNNKT (**P1−3A**). Note that Phe in **P1−3A** was not considered for substitution to ensure that the peptide will not migrate to the edges, yet still provide a reasonable assessment on the aromatic amino acids' relative importance. A relatively low mobility ($\mu = \Delta I_{DS}/C_{ox}d_s V_{DS}\Delta V_G$ (cm^2/(V s)), where d_S is the gate dielectric thickness, C_{ox} the gate oxide capacitance, and V_{DS} bias voltage) was noted from $\Delta I_{DS}/\Delta V_G$. Charge-transfer characteristics were not fully conclusive from Raman data, in comparison for example, to results by Das et al.[22] In this work, we improved the GFET devices with **P1** and **P1−3A** adsorption to minimize effects of environmental contamination by a careful annealing procedure, whereas a theoretical analysis on the electronic properties using a combination of methods provided insight into the device's intrinsic behavior.

At the same time, accurate prediction of peptide−graphene interactions and its effects on the electronic properties is still elusive. While use of empirical potentials for studying biological−carbon surfaces was reported, e.g., with CHARMM[20] or COMPASS,[23] complexity of prediction of adsorption of organic moieties on an inorganic surface was pointed out, for example, for adsorption of nucleobases on carbon nanotubes,[24] and using a polarizable force-field is advantageous. Detailed investigation of a hybrid material's interactions in a device setting is furthermore lacking. In this work, we applied a combined computational approach, whereby peptide adsorption was modeled by empirical molecular dynamics (MD) simulations, cross-checked with density functional theory (DFT). On the basis of the MD structure of the hybrid material system, we performed electronic structure and transport calculations, applying a nonequilibrium Green's function (NEGF) method. The large material model system necessitated use of the semiempirical density functional tight-binding (DFTB)[25] method, validated by DFT for a model His amino acid. Our results could explain, in part, effects of **P1**'s adsorption as a p-dopant in the device as dependent on residue type, and in particular the role of aromatic amino acid residues, while upon **P1−3A** adsorption, desorption of the Ala residues off the surface was qualitatively deduced from coarse-grain (CG) simulations, which would alter the doping effect of the peptide. However, as the electronic properties and transport depend on the details of the full peptide's adsorption on the graphene's surface, a conclusive understanding cannot as yet be attained. Our theoretical analysis on the intrinsic mechanism of doping single-layer graphene by aromatic amino-acid residues may be used to infer suppositions on peptide design for specific adsorption on the surface; however, elucidation of differences between various such residues as dependent on peptide composition will be considered in future work.

2. METHODS AND COMPUTATIONAL DETAILS

GFET Fabrication. Recent progress in large-scale graphene synthesis[26] and transfer[27] enables consistent fabrication of large area graphene-based devices. We used single-layer CVD graphene that was transferred to a prefabricated microelectrode pattern to form a GFET platform for testing the effect of peptide binding. A single-layer graphene coating was CVD grown on a Cu foil following a process described elsewhere.[26] Graphene was transferred from the Cu foil to the patterned electrode by using chemical etchants and thermal release tapes following the process of Bae et al.[27] Following a cleaning procedure described elsewhere,[28] the CVD GFET devices were annealed in 400 °C H$_2$/Ar mixture for 1 h to remove any organic residues from the transfer process. Patterns of 15 nm/35 nm Cr/Au electrodes were photolithographically fabricated on a silicon wafer with 1 μm thermal oxide using typical "lift-off" techniques, as described elsewhere.[29]

Peptide Binding to GFET. As described in a previous study,[20] the graphene region in the GFET was incubated with 100 μL of aqueous peptide (**P1** or **P1−3A**, 0.5 mg/mL) for 15 min followed by vigorous washing with DI water. Peptide adsorption on graphene was confirmed by AFM. GFET measurements were performed in an enclosed microprobe system after a 24 h 100 mtorr vacuum. Drain and source (DS) current (I_{DS}) was measured with applied −30 to 30 V gate voltage (V_{GS}) using a Keithley semiconductor characterization system model S4200.

MD and DFT Calculations. Atomic-level MD simulations were carried out using TINKER (version 5.1)[30] in the Canonical (NVT) ensemble at 298 K, using a Nose-Hoover thermostat.[31] The AMOEBAPRObio09 force-field[30] was used, in partnership with an additional, consistent set of parameters for modeling peptide adsorption on single-layer graphene.[32] AMOEBAPRO describes electrostatics via the distributed multipole approximation,[33,34] up to and including quadrupoles, and by inclusion of atom-based polarizabilities to model induction effects. Therefore, modeling of π-stacking between aromatic side-chains and the single-layer graphene surface is expected to be more appropriate in AMOEBAPRO than with other commonly available empirical force-fields.[32]

The Verlet[35] algorithm was used to solve Newton's equation of motion with an integration time step of 1 fs. A cutoff of 8 Å was applied for all nonbonded interactions. Long-range electrostatic interactions were evaluated using Ewald summations. The induction contributions were considered converged at a threshold of 0.0001 D. Because of computational considerations[36] a continuum implicit solvent model was used, namely ASP[37,38] with a modified background dielectric, previously found to yield physically reasonable behavior.[39,40] The single-layer graphene was modeled by a rigid sheet of 2772 carbon atoms, with approximate lateral dimensions of 77 × 86 (Å^2). **P1** was modeled in zwitterionic form with an N-terminal of NH$_3^+$ and a C-terminal of COO$^-$.

We explored eight different initial configurations, carrying out three MD runs per initial geometry, including both fully extended and random-coil arrangements of the peptide. The

random-coil conformations were taken from NVT simulations of the peptide alone, without the presence of the surface, with snapshots taken randomly from these trajectories. In each initial configuration, the peptide was brought close to the surface such that the backbone atoms were positioned roughly 5 Å above it, and was relaxed by energy minimization. The temperature was then increased gradually, where the system was first subjected to a short (5 ps) MD run at 198 K, followed by 50 ps at 230 K, before commencing simulation at 298 K. Each simulation was performed for ca. 3.5 ns, such that the fluctuations in the total potential energy converged to within 5% of the total value, and the distance between the key residues and the graphene surface settled to steady values (see Figure S1 in the Supporting Information), with both properties averaged over the last 0.5 ns of the run. Although the production simulation time does not appear long compared with conventional force-fields, it must be appreciated that AMOEBAPRO is considerably more expensive to implement, at least in serial form, occupying a territory between conventional force-fields and first-principles-based simulations.

CG MD simulations were performed using GROMACS (version 4.5.4).[41] The peptide was modeled with the MARTINI force-field,[42] where four carbon atoms were mapped to one uncharged (C1-type) to preserve their hexagonal symmetry, kept frozen during the simulation, to model single-layer graphene.[43] Peptide beads were first relaxed by geometry optimization, followed by MD simulation at 300 K in the gas-phase for 500 ns. Velocity rescaling with a stochastic term of 0.1 ps was used to regulate the temperature. A cutoff of 1.2 nm was used in calculating the Lennard-Jones 12−6 potential. Electrostatic interactions were evaluated with particle-mesh Ewald summations, using a short-range cutoff of 1 nm and relative strength of the Ewald-shifted direct potential of 1×10^{-5} at 1 nm (grid spacing of 0.12 nm, interpolation order of 6). The LINCS algorithm was chosen to reset bonds to their correct lengths after an unconstrained update.[44]

Based on the **P1-SLG** (single-layer graphene) model system, the graphene sheet size was reduced to 736 atoms for transport calculations. However, a lateral dimension of about 34×57 (Å^2) was maintained to ensure a relatively large distance between the peptide and its image (**P1$_{\text{AMOEBAPRO}}$-SLG**). To validate the use of **P1$_{\text{AMOEBAPRO}}$-SLG**, we also carried out gas-phase DFT geometry optimizations (**P1$_{\text{DFT}}$-SLG**). Periodic boundary conditions, with cubic cell dimensions large enough (ca. $30 \times 34 \times 57$ (Å^3)) to ensure that periodic images of the adsorbate do not interact, were applied. The single-layer graphene model was kept rigid, but unconstrained optimizations showed that the graphene was only slightly distorted from its planar conformation, and the supposition of a rigid graphene sheet justified. In calculations of individual amino acid model systems (**AA$_{\text{DFT}}$-SLG**), the graphene sheet consisted of 188 carbons, placed inside a simulation box of about $17 \times 19 \times 30$ (Å^3) dimensions, with three initial configurations used, differing by 45° rotations in the plane of the aromatic ring. The lowest-energy structures were selected for additional calculations. The termini of the amino acids were neutralized.

DFT geometry optimizations were performed using the all-electron QUICKSTEP method,[45] as implemented in CP2K.[46] The Becke97 functional[47] with a London dispersion correction developed by Grimme (B97-D)[48] and a 6-31G* basis set were applied. Geometry optimizations for the individual amino acids adsorbed on the graphene sheet were also performed using B97-D and the same basis set. Adsorption energies were obtained with counterpoise calculations performed with the same functional and basis set as geometry optimizations. Mulliken population analyses were also performed with CP2K.

Calculation of Electron Transport. The device model, mimicked by dividing the system into three regions, namely a left electrode (L), contact region (C), and a right electrode (R), was large, consisting of 1129 atoms (201 atoms-peptide, 736-SLG and 96 per/electrode; **P1$_{\text{Model}}$-SLG**), with dimensions 34 Å wide and 57 Å long in the central region, and 7.4 Å long for each electrode. For validation, a model system with His adsorption was also considered (**His-SLG**), having a total of 212 atoms.

Transport calculations were performed using a NEGF method[49] with the Landauer−Buttiker assumptions.[50,51] The Green's function **G** can be written as

$$\begin{pmatrix} \mathbf{H}_L + \mathbf{\Sigma}_L & \mathbf{V}_L & 0 \\ \mathbf{V}_L{}^\dagger & \mathbf{H}_C & \mathbf{V}_R \\ 0 & \mathbf{V}_R{}^\dagger & \mathbf{H}_R + \mathbf{\Sigma}_R \end{pmatrix}$$

where $\mathbf{H}_L$, $\mathbf{H}_C$, and $\mathbf{H}_R$ are the Hamiltonian matrices in regions L, C, and R, respectively; $\mathbf{V}_L(\mathbf{V}_R)$ represent the interaction between the L(R) and C regions, and $\sum_L$ and $\sum_R$ are the self-energies extracted from a calculation of the bulk phase. From the Green's function the density matrix is obtained, used to calculate $\mathbf{V}_L(\mathbf{V}_R)$ and $\mathbf{H}_C$, depending on the nonequilibrium electron density, and the scheme completed to self-consistency. Under an applied bias (V_b) the chemical potentials μ shift as $\mu_L(V_b) = \mu_L(0) + eV_b/2$ and $\mu_R(V_b) = \mu_R(0) - eV_b/2$, where $\mu_L(0)$ and $\mu_R(0)$ represent the chemical potentials at zero bias on the L and R electrodes, respectively. The total transmission is $T(E) = \text{Tr}[\mathbf{t}\mathbf{t}^\dagger]$, where $\mathbf{t}(E) = [\mathbf{\Gamma}_R(E)]^{1/2} \mathbf{G}(E)[\mathbf{\Gamma}_L(E)]^{1/2}$, and $\mathbf{\Gamma}_R$ and $\mathbf{\Gamma}_L$ the contact broadening for the L and R electrodes. The current is given by

$$I(V) = \frac{2e}{h} \int_{-\infty}^{\infty} [f[E - \mu_L] - f[E - \mu_R]]T(E)dE; f[E - \mu]]$$

$$= \frac{1}{1 + \exp\left[E - \dfrac{\mu}{k_B T}\right]}$$

Transport calculations were performed using ATK.[52] A double-ζ with polarization (DZP) basis set and PBE functional[53] for the small model system of His adsorbed on single-layer graphene was used. For consistency, a dispersion-corrected functional was not used in this case because of lack of a dispersion correction in DFTB we applied in ATK. However, note that no structure optimization was involved and the transport calculations were based on a structure generated from MD simulations. For DFTB, extended Hückel (EH),[54] Cerda's parameters for C,[55] and Hoffmann's[56,57] and Müller[52] parameters for H, N, O were tested. CP2K parameters provided in ATK[52] and Mio-0-1 Slater−Koster parameters[25] were tested at zero bias. For the His model, a Monkhorst−Pack k-points grid of $1 \times 9 \times 9$ was used to sample Brillouin zone in the SCF step and a k-points grid of 1×50 for DOS and transmission calculations. For the peptide-graphene device model systems, k-point grids of $1 \times 3 \times 3$ and $1 \times 1 \times 50$ in the SCF step and density of states (DOS) and transmission calculations, respectively, were used. Effects of gold leads were modeled using Transiesta,[51] with PBE and a DZP basis set for

7472

dx.doi.org/10.1021/am401731c | ACS Appl. Mater. Interfaces 2013, 5, 7470−7477

C and SZP for Au. A summary of computational methods used in this work is given in Table S1 in the Supporting Information.

3. RESULTS AND DISCUSSION

Peptide Adsorption on a Single-Layer Graphene Surface. In the empirical all-atom MD simulations, the relative average energies of the top 5 final trajectories were 0.0, 3.8, 5.6, 6.5, and 7.3 kcal/mol. The lowest energy configuration was used in subsequent calculations (**P1**$_{AMOEBAPRO}$-**SLG**). Derivation of the lowest energy configuration of model system **P1−3A**$_{AMOEBAPRO}$-**SLG** followed a similar protocol. Because of the annealing of the device in vacuum after initial adsorption, peptide structures were thereafter assumed to feature charge-neutral N- and C-termini, modeled as NH_2 and COOH, respectively. To ensure that no meaningful changes were introduced upon neutrality and also assess the adsorption on the surface during a longer simulation time, CG simulations were performed for model systems **P1**$_{AMOEBAPRO}$-**SLG** and **P1−3A**$_{AMOEBAPRO}$-**SLG** for 500 ns.

The lowest-energy **P1**$_{AMOEBAPRO}$-**SLG** configuration is shown in Figure 1, demonstrating partial stacking of aromatic amino
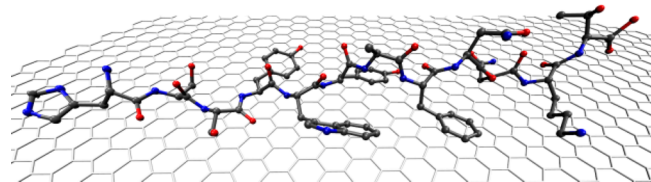

Figure 1. Optimized structure of the lowest energy configuration of system model **P1−3A**$_{AMOEBAPRO}$-**SLG**. Details of the structural parameters are described in the text. For clarity, hydrogen bonds were removed and all bonds are shown as single.

acids on the single-layer graphene surface. Indeed, noncovalent functionalization of graphene by $\pi-\pi$ interactions has proven an important driving force in nanoscience.[58] Adsorption characteristics for the residues in **P1**$_{AMOEBAPRO}$-**SLG** are summarized in Table 1, along with results for **P1**$_{DFT}$-**SLG** and individual amino acids. In the lowest energy configuration of **P1**$_{AMOEBAPRO}$-**SLG** π-stacking occurs for Phe/8 and Tyr/6, yet in considering fluctuations and the average behavior of the residues (see Figure S1 in the Supporting Information), π-stacking for all aromatic amino acids can generally be assumed.[20] Regarding **P1−3A**$_{AMOEBAPRO}$-**SLG** (details on the changes in the configuration in this case are summarized in Table S2 in the Supporting Information), Phe is not stacked on the surface, and the angle between the surface of the graphene

sheet and aromatic ring's plane (α) is ca. 53°. The relative orientation of the aromatic residues to the surface has not changed significantly upon DFT optimization, although stacking for Tyr/6 and Phe/8 slightly improved. Distances of the aromatic ring for Tyr/6 and Phe/8 have also been reproduced in the calculations for **P1**$_{DFT}$-**SLG** (see Table 1). This further confirms applicability of AMOEBAPRO-based structures for calculating electron transport.

Because of increased structural fluctuation for the end amino acid residues in the peptide, we discuss the results only for Phe in comparing adsorption for **P1** and **P1−3A** using AMOE-BAPRO. The ring of Phe tilted away from its relatively parallel orientation to the graphene surface in **P1−3A**, and the centroid distance from the ring increased by almost 2 Å, finding a cooperative π−stacking effect between Tyr/6 and Ph/8 in **P1**. On the other hand, the **P1−3A** peptide came closer to the surface overall. For example, the average distance of the peptide-group atoms to the surface in **P1**$_{AMOEBAPRO}$-**SLG** was 5.3 Å, whereas a value of 4.3 Å was calculated for **P1−3A**$_{AMOEBAPRO}$-**SLG** (see Table S1 in the Supporting Information). Averaging over all atoms resulted in distances of 4.9 and 4.3 Å for **P1**$_{AMOEBAPRO}$-**SLG** and **P1−3A**$_{AMOEBAPRO}$-**SLG**, respectively. This could be explained by partial unwinding of **P1−3A** on the surface, hence moving the backbone closer to it, as is demonstrated by the angles between the peptide-group and graphene planes (see Table S1 in the Supporting Information). Calculated adsorption energies for **P1**$_{AMOEBAPRO}$-**SLG** and **P1−3A**$_{AMOEBAPRO}$-**SLG**, 3.31 and 3.24 eV (using B97-D), respectively, are consistent with previous work on a weakly adsorbed moiety on graphene.[59] Our quartz crystal microbalance (QCM) experiments for the graphene-peptide adsorbed systems confirmed a similar number of adsorbed peptide molecules for both **P1** and **P1−3A** (see Figure S2 in the Supporting Information). However, note that because of potential substrate effects, experimental observations for the two peptides may not capture the intrinsic adsorption properties. Assembly of the **P1** and **P1−3A** peptides on the surface, leaving unique pores due to the evaporation of the entrapped water, is shown by atomic force spectroscopy (AFM) images in Figure S3 in the Supporting Information. Differences in pore-density and size are noticeable for the two peptides, but a full interpretation is beyond the scope of this study.

To gain an understanding of aromatic amino acids' intrinsic adsorption on single-layer graphene, we investigated adsorption of individual amino acids. Results for the **AA**$_{DFT}$-**SLG** model systems demonstrated π-stacking of the aromatic residues on the surface ($\alpha \leq 4°$ in all cases, Table 1), consistent with the work of Rajesh et al.[60] on adsorption of the aromatic side-

Table 1. Centroid Distances, Measured from the Centroid of the Aromatic Ring to the Graphene Plane (D_c, Å), Angle between the Planes of the Aromatic Ring and the Graphene Surface (α°), and Mulliken Charges (MC, e)[c] for P1$_{AMOEBAPRO}$**-SLG**[b]**, P1**$_{DFT}$**-SLG, and AA**$_{DFT}$**-SLG optimized structures**[a]

aromatic residue in peptide/sequence number	P1$_{AMOEBAPRO}$-SLG			P1$_{DFT}$-SLG			AA$_{DFT}$-SLG			
	D_c	α	MC[c]	D_c	MC[c]	α		D_c	α	MC[c]
His/1	4.642 (3.446)[b]	27.7 (18.3)[b]	0.033	4.353	0.034	33.0	His	3.395	4.0	−0.005
Tyr/4	3.879	23.1	0.004	3.681	0.010	18.4	Tyr	3.455	2.9	−0.028
Trp/5	4.061	30.7	0.041	4.095	0.025	28.7	Trp	3.362	3.4	−0.001
Tyr/6	3.360	9.3	−0.046[d]	3.363	−0.027[d]	5.5	Tyr	3.455	2.0	−0.028
Phe/8	3.441 (5.015)[b]	9.1 (53.3)[b]	−0.090[d]	3.477	−0.033[d]	6.4	Phe	3.577	1.9	−0.012

[a]Details of methods applied for the different structures is given in the text. [b]Results for **P1−3A**$_{AMOEBAPRO}$-**SLG**. [c]Mulliken population analyses are shown only for stacked residues. [d]Negative MC results for aromatic residues with small α and $D_c < 3.5$ Å, indicating $\pi-\pi$ stacking.

chains' rings of His, Phe, Tyr, and Trp on single-layer graphene. It was shown that the aromatic rings oriented parallel to the surface with average interplanar distances of 3.21, 3.33, 3.34 and 3.50 Å,[60] and similarly by Czyznikowska et al.[61] These results, as expected, are different than our calculated distances, of 3.10 ± 0.07, 3.40 ± 0.02, 3.12 ± 0.05, 3.35 ± 0.06 Å, evaluated by averaging the shortest distances between the single-layer graphene plane and the heavy atoms in the rings, and also with centroid distances, measured from the centroid of the aromatic ring to the single-layer graphene plane (see Table 1).

Adsorption energies follow the trend His < Phe < Tyr < Trp, with values of −8.9, −9.8, −13.3, −15.1 kcal/mol for His, Phe, Tyr, and Trp, respectively, as compared to −4.8, −5.8, −7.1, and −9.7 kcal/mol values previously reported,[60] respectively, however not taking into account the geometry of the amino acid and only the aromatic ring's adsorption on the surface, as well as due to the lack of inclusion of London dispersion interactions in the functional. Krishtal et al.[62] have shown that calculated polarizabilites of the amino acids also follow this trend for the side chains but not for the backbone, although the overall values are proportional to the corresponding values of the residues' side-chains. This is an important consideration in simulation of peptide-graphene interactions not taken into account previously,[60,61] to be further explored in future work.

Device Characteristics. As mentioned, electron transport calculations are computationally intensive, beyond the realm of first principles for the systems studied here, and therefore the semiempirical DFTB approach was undertaken, as described in the Methods and Computational Details section, except for a (**His**-**SLG**) model system, which was considered with DFT for validation of the parameters used in DFTB (summary of results and discussion is given in Figure S4 in the Supporting Information). On the basis of these results, the Mio-0−1 parameters were used for analysis of the electronic properties of the **P1$_{Model}$**-**SLG** device. First, we assess the contribution of the residues comprising the **P1** peptide. PDOS of **P1$_{Model}$**-**SLG** (see Figure 2a) indicate strong coupling of the adsorbate's filled states with those of the graphene valence band. The local DOS reveal that the high peaks of **P1**, located at 1.4 and 2.0 eV, below the Fermi level, are due primarily to contribution of aromatic amino acids (Figure 2b). Thus, the **P1−3A** peptide at least partially provides an assessment of the effects of the aromatic amino acids.

Experimentally, we note different behavior in the GFET upon **P1** and **P1−3A** adsorption (see Figure 3). Initially, water, **P1**, and **P1−3A** are shown to cause further p-doping of the single-layer graphene that is already p-doped without adsorbates. After annealing in vacuum the water content is minimized and the device shows similar behavior to a nonadsorbed device, whereas **P1** is still strongly p-doping upon elimination of water. This observation implies little interaction of water molecules with the peptide adsorbate. On the other hand, **P1−3A** adsorption causes n-doping of the nonadsorbed device (Figure 3). Note that there is a slight change in the slope of I_{DS} vs V_{GS} in the **P1−3A** adsorbed device, which demonstrates a slight decrease in mobility.

To further understand the difference between devices with **P1** and **P1−3A** adsorption, the nature of charge transfer was analyzed. Charge transfer in the **P1$_{AMOEBAPRO}$**-**SLG** model system under zero bias indicated weak p-doping of the graphene sheet (+0.008e, obtained using DFTB/Mio-0−1 parameters), increasing under bias to +0.013 and +0.011e for
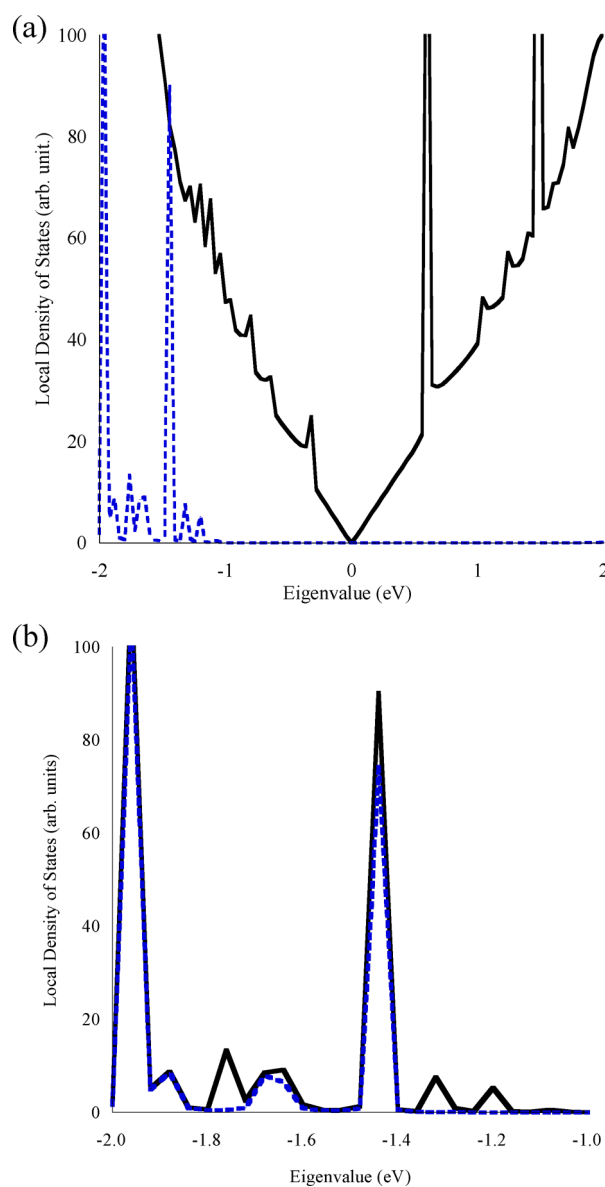

Figure 2. (a) Local DOS obtained with DFTB calculations using Mio-0−1 parameters for single-layer graphene model (solid black line) and **P1** in **P1-SLG** (blue dashed line); (b) where **P1** (solid black line) and the contribution of aromatic residues (blue dashed line) are indicated.

1.0 and 2.0 V, respectively. The value is small as expected, in comparison to strong electron-acceptors,[63] consistent with the small blue shift of 1.7 cm^{-1} in the 2D mode observed for **P1**-**SLG**.[20] However, **P1−3A$_{AMOEBAPRO}$**-**SLG** was also shown to cause p-doping, with charge transfer of +0.026e under zero bias, implying behavior as an electron-acceptor. Indeed, electron transport calculations (see Figure S5 in the Supporting Information) demonstrate that the transmission is almost identical for the two peptides adsorbed on graphene. To ensure validity of these results, we compare to Mulliken partial atomic charges calculated for the model systems **P1$_{AMOEBAPRO}$**-**SLG** and **P1−3A$_{AMOEBAPRO}$**-**SLG** using DFT (described in the Methods and Computational Details section), which also indicate p-doping (+0.120e and +0.163e for **P1$_{AMOEBAPRO}$**-**SLG** and **P1−3A$_{AMOEBAPRO}$**-**SLG**, respectively, Table S3 in the Supporting Information).

(a)   (b)
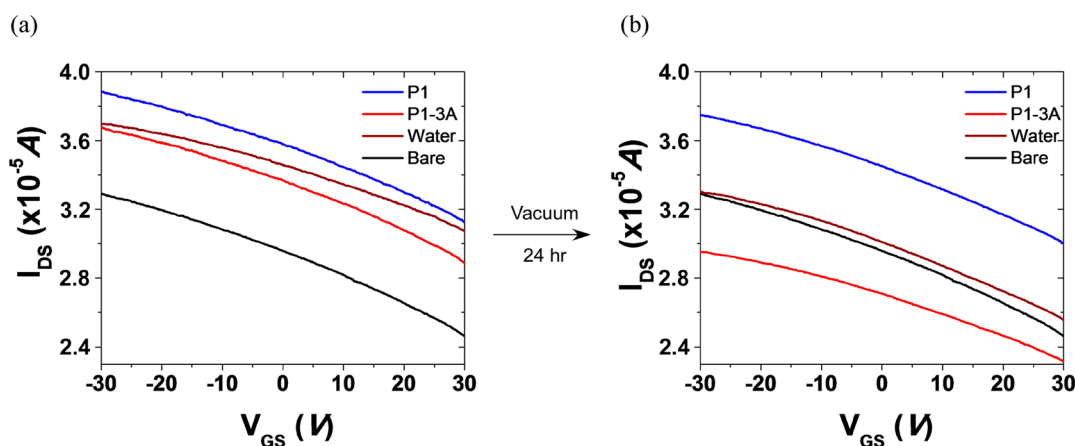

Figure 3. P1, P1−3A, and water adsorption effects on bare GFET characteristics (a) before and (b) after 24 h vacuum at 100 mtorr.

Overall, we note that the π-stacked aromatic residues in **P1** especially cause intrinsic p-doping of single-layer graphene. On the other hand, in the MD atomistic simulations **P1−3A** unwinds and gets closer to the surface, thus causing p-doping by the backbone's proximity to graphene. The large experimentally observed p-doping could be due to larger coverage on the surface than by a single peptide and to interaction with the electrodes. Indeed, on the basis of an analytical model that describes the Fermi-level shift in graphene in terms of the metal's work function, Khomyakov et al.[64] have shown that Au would cause p-doping of graphene. Similarly, in our calculations on a device with graphene adsorbed on Au(111) leads (see Figure S6a in the Supporting Information), p-doping of the graphene was demonstrated, where the transmission spectrum of graphene with gold leads exhibited a shift of the Dirac point toward the conduction band of the graphene (see Figure S6b in the Supporting Information). This behavior is noted for a graphene-gold distance of 3.6 Å, consistent with previous work that demonstrated p-doping for distances ranging from 3.3 to 5.0 Å.[64]

The response for **P1−3A**, however, is not consistent with our charge transfer calculations. To gain a qualitative understanding of changes in **P1−3A**'s distance to the single-layer graphene surface over a longer simulation time not captured by the atomistic simulations, equilibrated CG MD simulations were analyzed. Interestingly, using the last 100 of the 500 ns simulation, average distances of the backbone beads of Tyr/4, Trp/5, Tyr/6 in **P1** to the graphene surface in **P1-SLG** were approximately 4.5, 4.8, and 4.7 Å, respectively, consistent with the atomistic AMOEBAPRO atomistic force-field results and therefore showing that the interactions between the peptide and graphene surface can be captured qualitatively by the MARTINI force-field. For **P1−3A-SLG**, the corresponding values for Ala/4, Ala/5, Ala/6 changed to 8.8., 9.1, and 8.3 Å, respectively, also showing significant fluctuations (see Figure S7 in the Supporting Information). This could result in different adsorption and changes in charge transfer, possibly leading to better agreement with experiment. However, differences with experimental observations could also be due to environmental or substrate effects in the device, and from defects in the graphene samples.

4. CONCLUSION

In conclusion, using a combined computational approach, we suggest that the experimentally observed p-doping by the adsorbed **P1** peptide in a GFET device may be due in part to an intrinsic doping mechanism, as compared to **P1−3A** with substitution of three aromatic amino acid residues by Ala. Peptide adsorption was investigated using atomistic MD simulations with an empirical potential parametrized for carbon surfaces and further validated for the lowest energy configuration by DFT with a London dispersion corrected functional. Charge transfer and electron transport calculations applying a NEGF method with DFTB, based on the lowest energy structure of the hybrid material system, suggest that π−π stacking of the aromatic residues and proximate backbone on the graphene surface in **P1** may have a role in the p-doping. p-Type doping could be affected also by the gold leads as we explained, substrate, device, or environmental effects not taken into account in the simulations.

Interestingly, upon substitution of three of the aromatic amino acid residues to Ala in **P1−3A**, a transition from p- to n-doping was observed experimentally as compared to the nonadsorbed device, yet not explained based on the atomistic MD simulation structures. To gain a qualitative understanding of **P1−3A**'s adsorption on single-layer graphene over a much longer simulation time, which may differ from aromatic residues' swift anchoring on the surface for **P1**, we analyzed equilibrated CG simulations. Desorption of Ala residues from the surface was shown, which in turn may result in altered charge transfer characteristics. Overall, the combination of methods we used enabled us to suggest, in part, suppositions on the structural, electronic, and electron-transport properties in a GFET with peptide adsorption, which in turn may assist in providing suggestions for design of specific peptide adsorption in GFET applications.

■ ASSOCIATED CONTENT

Ⓢ Supporting Information

Geometrical parameters for the peptide backbone and graphene, Mulliken partial atomic charges, distances between the peptide residues during atomic-level and CG MD, QCM frequency change for graphene upon exposure to peptides, AFM images, discussion of results and DOS for the **SLG-His** model, and transmission results for peptide adsorbed on single-layer graphene. This material is available free of charge via the Internet at http://pubs.acs.org.

■ AUTHOR INFORMATION

Corresponding Author

*E-mail: Brahim.Akdim@wpafb.af.mil (B.A.); Ruth.Pachter@wpafb.af.mil (R.P.).

Notes

The authors declare no competing financial interest.

■ REFERENCES

(1) Dan, Y.; Lu, Y.; Kybert, N. J.; Luo, Z.; Johnson, A. T. C. *Nano Lett.* **2009**, 9, 1472−1475.

(2) Cooper, D. R.; D'Anjou, B.; Ghattamaneni, N.; Harack, B.; Hilke, M.; Horth, A.; Majlis, N.; Massicotte, M.; Vandsburger, L.; Whiteway, E.; Yu, V. *ISRN Condens. Mater. Phys.* **2012**, 501686, 56.

(3) Adam, S. *Graphene Carrier Transport Theory Graphene Nanoelectronics*; Raza, H., Ed.; Springer: Berlin, 2012; pp 357−394.

(4) Wehling, T. O.; Katsnelson, M. I.; Lichtenstein, A. I. *Chem. Phys. Lett.* **2009**, 476, 125−134.

(5) Fan, X. F.; Zheng, W. T.; Chihaia, V.; Shen, Z. X.; Kuo, J.-L. *J. Phys.: Condens. Mat.* **2012**, 24, 305004/1−305004/10.

(6) Chen, K.; Wang, X.; Xu, J.-B.; Pan, L.-J.; Wang, X.-R.; Shi, Y. *J. Phys. Chem. C* **2012**, 116, 6259−6267.

(7) Miwa, R. H.; Schmidt, T. M.; Scopel, W. L.; Fazzio, A. *Appl. Phys. Lett.* **2011**, 99, 163108/1−163108/3.

(8) Shin, D.-W.; Lee, H. M.; Yu, S. M.; Lim, K.-S.; Jung, J. H.; Kim, M.-K.; Kim, S.-W.; Han, J.-H.; Ruoff, R. S.; Yoo, J.-B. *ACS Nano* **2012**, 6, 7781−7788.

(9) Chan, J.; Venugopal, A.; Pirkle, A.; McDonnell, S.; Hinojos, D.; Magnuson, C. W.; Ruoff, R. S.; Colombo, L.; Wallace, R. M.; Vogel, E. M. *ACS Nano* **2012**, 6, 3224−3229.

(10) Adam, S.; Hwang, E. H.; Galitski, V. M.; Das, S. S. *Proc. Natl. Acad. Sci. U.S.A.* **2007**, 104, 18392−18397.

(11) Liang, X.; Fu, Z.; Chou, S. Y. *Nano Lett.* **2007**, 7, 3840−3844.

(12) Romero, H. E.; Shen, N.; Joshi, P.; Gutierrez, H. R.; Tadigadapa, S. A.; Sofo, J. O.; Eklund, P. C. *ACS Nano* **2008**, 2, 2037−2044.

(13) Kumar, B.; Min, K.; Bashirzadeh, M.; Farimani, A. B.; Bae, M. H.; Estrada, D.; Kim, Y. D.; Yasaei, P.; Park, Y. D.; Pop, E.; Aluru, N. R.; Salehi-Khojin, A. *Nano Lett.* **2013**, 13, 1962−1968.

(14) Cheng, Z.; Zhou, Q.; Wang, C.; Li, Q.; Wang, C.; Fang, Y. *Nano Lett.* **2011**, 11, 767−771.

(15) Nagashio, K.; Yamashita, T.; Nishimura, T.; Kita, K.; Toriumi, A. *J. Appl. Phys.* **2011**, 110, 024513/1−024513/6.

(16) Cui, Y.; Kim, S. N.; Naik, R. R.; McAlpine, M. C. *Acc. Chem. Res.* **2012**, 45, 696−704.

(17) Nguyen, P.; Berry, V. *J. Phys. Chem. Lett.* **2012**, 3, 1024−1029.

(18) Schedin, F.; Geim, A. K.; Morozov, S. V.; Hill, E. W.; Blake, P.; Katsnelson, M. I.; Novoselov, K. S. *Nat. Mater.* **2007**, 6, 652−655.

(19) Sharf, T.; Kevek, J. W.; DeBorde, T.; Wardini, J. L.; Minot, E. D. *Nano Lett.* **2009**, 12, 6380−6384.

(20) Kim, S. N.; Kuang, Z.; Slocik, J. M.; Jones, S. E.; Cui, Y.; Farmer, B. L.; McAlpine, M. C.; Naik, R. R. *J. Am. Chem. Soc.* **2011**, 133, 14480−14483.

(21) Pender, M. J.; Sowards, L. A.; Hartgerink, J. D.; Stone, M. O.; Naik, R. R. *Nano Lett.* **2006**, 6 (1), 40−44.

(22) Das, A.; Pisana, S.; Chakraborty, B.; Piscanec, S.; Saha, S. K.; Waghmare, U. V.; Novoselov, K. S.; Krishnamurthy, H. R.; Geim, A. K.; Ferrari, A. C.; Sood, A. K. *Nat. Nanotechnol.* **2008**, 3, 210−215.

(23) Trohalaki, S.; Pachter, R.; Luckarift, H. R.; Johnson, G. R. *Fuel Cells* **2012**, 12, 656−664.

(24) Akdim, B.; Pachter, R.; Day, P. N.; Kim, S. S.; Naik, R. R. *Nanotechnology* **2012**, 23, 165703/1−165703/6 S165703/1-S165703/4.

(25) Elstner, M.; Porezag, D.; Jungnickel, G.; Elsner, J.; Haugk, M.; Frauenheim, T.; Suhai, S.; Seifert, G. *Phys. Rev. B* **1998**, 58, 7260−7268.

(26) Li, X.; Cai, W.; An, J.; Kim, S.; Nah, J.; Yang, D.; Piner, R.; Velamakanni, A.; Jung, I.; Tutuc, E.; Banerjee, S. K.; Colombo, L.; Ruoff, R. S. *Science* **2009**, 324 (5932), 1312−1314.

(27) Bae, S.; Kim, H.; Lee, Y.; Xu, X.; Park, J.-S.; Zheng, Y.; Balakrishnan, J.; Lei, T.; Ri Kim, H.; Song, Y. I.; Kim, Y.-J.; Kim, K. S.; Ozyilmaz, B.; Ahn, J.-H.; Hong, B. H.; Iijima, S. *Nat. Nanotechnol.* **2010**, 5 (8), 574−578.

(28) Ishigami, M.; Chen, J. H.; Cullen, W. G.; Fuhrer, M. S.; Williams, E. D. *Nano Lett.* **2007**, 7 (6), 1643−1648.

(29) Slocik, J. M.; Kim, S. N.; Whitehead, T. A.; Clark, D. S.; Naik, R. R. *Small* **2009**, 5 (18), 2038−2042.

(30) Ponder, J. W.; Ren, P.; Pappu, R. V.; Hart, R. K.; Hodgson, M. E.; Cistola, D. P.; Kundrot, C. E.; Richards, F. M.; *TINKER*, Version 5.1; Washington University School of Medicine: St. Louis, MO.

(31) Nose, S. *Mol. Phys.* **1984**, 52, 255−68.

(32) Walsh, T. R. *Mol. Phys.* **2008**, 106, 1613−1619.

(33) Stone, A. J. *Chem. Phys. Lett.* **1981**, 83, 233−9.

(34) Stone, A. J.; Alderton, M. *Mol. Phys.* **1985**, 56, 1047−64.

(35) Verlet, L. *Phys. Rev.* **1967**, 159, 98−103.

(36) Walsh, T. R.; Liang, T. *J. Comput. Chem.* **2009**, 30, 893−9.

(37) Eisenberg, D.; McLachlan, A. D. *Nature* **1986**, 319, 199−203.

(38) Wesson, L.; Eisenberg, D. *Protein Sci.* **1992**, 1, 227−35.

(39) Tomasio, S. D.; Walsh, T. R. *Mol. Phys.* **2007**, 105, 221−229.

(40) Tomasio, S. M.; Walsh, T. R. *J. Phys. Chem. C* **2009**, 113, 8778−8785.

(41) Hess, B.; Kutzner, C.; van der Spoel, D.; Lindahl, E. *J. Chem. Theory Comput.* **2008**, 4 (3), 435−447.

(42) Monticelli, L.; Kandasamy, S. K.; Periole, X.; Larson, R. G.; Tieleman, D. P.; Marrink, S.-J. *J. Chem. Theory Comput.* **2008**, 4 (5), 819−834.

(43) Wu, D.; Yang, X. *J. Phys. Chem. B* **2012**, 116, 12048−12056.

(44) Hess, B.; Bekker, H.; Berendsen, H. J. C.; Fraaije, J. G. E. M. *J. Comput. Chem.* **1997**, 18 (12), 1463−1472.

(45) VandeVondele, J.; Krack, M.; Mohamed, F.; Parrinello, M.; Chassaing, T.; Hutter, J. *Comput. Phys. Commun.* **2005**, 167, 103−128.

(46) CP2K. http://www.cp2k.org/.

(47) Becke, A. D. *J. Chem. Phys.* **1997**, 107, 8554−8560.

(48) Grimme, S. *J. Comput. Chem.* **2006**, 27, 1787−1799.

(49) Brandbyge, M.; Mozos, J.-L.; Ordejon, P.; Taylor, J.; Stokbro, K. *Phys. Rev. B* **2002**, 65, 165401/1−165401/17.

(50) Buttiker, M.; Imry, Y.; Landauer, R. *Phys. Rev. B* **1985**, 31, 6207/15.

(51) Stokbro, K.; Taylor, J.; Brandbyge, M.; Ordejon, P. *Ann. N.Y. Acad. Sci.* **2003**, 1006, 212−226.

(52) *Atomistix Toolkit version 12.2*; QuantumWise: Copenhagen, Denmark; http://www.quantumwise.com/.

(53) Perdew, J. P.; Burke, K.; Ernzerhof, M. *Phys. Rev. Lett.* **1996**, 77, 3865−3868.

(54) Stokbro, K.; Petersen, D. E.; Smidstrup, S.; Blom, A.; Ipsen, M.; Kaasbjerg, K. *Phys. Rev. B* **2010**, 82, 075420/1−075420/7.

(55) Cerda, J.; Soria, F. *Phys. Rev. B* **2000**, 61, 7965−7971.

(56) Whangbo, M.-H.; Hoffmann, R. *J. Chem. Phys.* **1978**, 68, 5498−500.

(57) Ammeter, J. H.; Buergi, H. B.; Thibeault, J. C.; Hoffmann, R. *J. Am. Chem. Soc.* **1978**, 100, 3686−92.

(58) Dougherty, D. A.; Stauffer, D. A. *Science (Washington, D. C., 1883-)* **1990**, 250, 1558−60.

(59) Peimyoo, N.; Yu, T.; Shang, J.; Cong, C.; Yang, H. *Carbon* **2012**, 50, 201−208.

(60) Rajesh, C.; Majumder, C.; Mizuseki, H.; Kawazoe, Y. *J. Chem. Phys.* **2009**, 130, 124911/1−124911/6.

(61) Czyznikowska, Z.; Bartkowiak, W. *J. Comput. Chem.* **2011**, 32, 1887−1895.

(62) Krishtal, A.; Senet, P.; Van, A. C. *J. Chem. Phys.* **2009**, 131, 044312/1−044312/11.

7476

dx.doi.org/10.1021/am401731c | *ACS Appl. Mater. Interfaces* 2013, 5, 7470−7477

(63) Dong, X.; Fu, D.; Fang, W.; Shi, Y.; Chen, P.; Li, L.-J. *Small* **2009**, *5*, 1422−1426.

(64) Khomyakov, P. A.; Giovannetti, G.; Rusu, P. C.; Brocks, G.; van den Brink, J.; Kelly, P. J. *Phys. Rev. B* **2009**, *79* (19), 195425.